

# Novel ENG metamaterial for Gain enhancement of an off-set fed CPW Concentric circle shaped patch antenna

Sujatha Priyadharshini A (✉ [sujatharsauice@gmail.com](mailto:sujatharsauice@gmail.com))

PITS: Parisutham Institute of Technology and Science <https://orcid.org/0000-0001-5869-5472>

C. Arvind

Karpagam College of Engineering

Madurakavi Karthikeyan

Vellore Institute of Technology: VIT University

---

## Research Article

**Keywords:** Metamaterial Antenna, near zero refractive index (NZRI), ENG metamaterial, DNG metamaterial, wideband antenna, high gain antennas

**Posted Date:** June 14th, 2022

**DOI:** <https://doi.org/10.21203/rs.3.rs-1607826/v1>

**License:**  This work is licensed under a Creative Commons Attribution 4.0 International License.

[Read Full License](#)

---

**Version of Record:** A version of this preprint was published at Wireless Personal Communications on April 3rd, 2023. See the published version at <https://doi.org/10.1007/s11277-023-10390-8>.

# Abstract

This paper presents a multiband coplanar waveguide (CPW)-fed concentric circle shaped patch antenna for WLAN, LTE-A, 5G Wi-Fi, and X-band applications, which is loaded with metamaterial unit cell. The proposed patch antenna employs arc shaped patch and concentric circle shaped patch achieves ultra-wideband operation. The proposed two layer antenna configuration consists of metamaterial super-substrate. The measured reflection co-efficient ( $S_{11}$ ) demonstrated three wideband operation ranging from 3.06GHz – 4.72GHz (B.W of 42%), 4.94GHz-6.19GHz (B.W of 22%) and 6.50 GHz – 10.56 GHz (B.W of 47.5%). The metamaterial structure is obtained through the arrangement of the proposed unit cell in  $5 \times 5$  order. The proposed metamaterial structure properties were examined for wave propagation through the material in two major axes directions (x and y-axis). For both axis, the metamaterial exhibits near Zero refractive index for wide range of frequency. The addition of this super-substrate provides significant gain enhancement by 181% when the maximum gain reaches 6.2 dBi at X-band frequency. Since the proposed antenna is more efficient, it might be used for X-band operations such as satellite communication, military, and medical monitoring.

## I Introduction

In today's technology world, there is a tremendous demand for highly efficient, low-cost, multi-standard operational antennas with a compact size and high gain [1–4]. Metasurface (MS) structures have recently been used to modify incident electromagnetic waves in both the optical and microwave frequency domains [2–5]. With applications in satellite and terrestrial communications, radar, imaging, and wireless power transfer, the metasurface concept has evolved as an effective technique for accomplishing gain enhancement, beam forming, and wave-front shaping [6]. Metasurface are two-dimensional configurations of sub wavelength scatterers that influence electromagnetic wave propagation [7–8]. The incident electromagnetic wave's resonant effects are controlled by the MS structure, which is made up of unit cells [9]. At the C, S, and X band frequencies, many metamaterials with double negative (DNG) medium properties have been observed [10–11]. These materials are combined with the conventional patch antenna to enhance its performance in terms of gain, beam forming etc. In [12, 13], the MS antenna with a superstrate construction has been devised to boost gain in the X band region.

For ultra-wideband applications, a compact antenna with capacitance-loaded strip unit cell with negative refractive index and SRR was presented in [14]. At 10.15 GHz, the antenna had the greatest gain of 5.16 dBi. Periodic array structure [15], spiral resonator [16], complementary split ring resonator (CSRRs) [17] and split-ring resonator [18] are just a few of the metamaterial topologies that have been described and used to improve the patch antenna's performance. For example, SRR-based unit cell topologies have been investigated for creating multi-band functioning, minimizing antenna size, and boosting gain. However, these DNG metamaterial enhances the gain only in particular frequency region. There have also been proposals of mu-negative metamaterial (MNG) and epsilon negative metamaterial (ENG) [19–20]. Additionally, some of these materials exhibit the properties of near zero refractive index (NZRI)[21]. The

NZRI metamaterials are capable of enhancing antenna gain across the whole operating band. In [22], the metamaterial super-substrate with near zero refractive index has been proposed for the antenna size of  $78.6 \text{ mm} \times 42.5 \text{ mm}$  and achieved gain enhancement in four bands of operation. However, the size of the antenna is very large. By embedding split ring resonator (SRR) and complementary SRR structures with composite right/left handed metamaterial, an antenna's gain is increased in [23]. Furthermore, different metamaterial-loaded multiband antennas have been reported in [24–25], featuring trade-off characteristics such as size, number of operating bands and gain.

We present a novel antenna with a concentric circular shaped patch that is supported by an ENG metamaterial loaded super-substrate in this work. The gain is increased over a wider operating band with this arrangement. The structure of the paper is outlined as follows. Section II describes the structure and operation of the unit cell. The proposed antenna structure and its evolution are discussed in Section III. The modelling and experiment results are discussed in Section IV. This paper concludes in Section V.

## I i Unit Cell Structure

The performance of a traditional antenna has been improved by the addition of a unique metasurface. The MS layer was built up atop a 0.8 mm thick FR-4 dielectric that lay beneath the patch antenna. The metasurface is made up of unit cells that are spaced at regular intervals. Figure 1 depicts the proposed unit cell, while Table 1 lists the appropriate dimensions. As seen in Fig. 1, the unit cell consists of an L-shaped patch in the centre surrounded by a slotted square shaped patch. The proposed unit cell is made from a FR-4 substrate with a dielectric constant of 4.6 and a thickness of 0.8 mm. The metasurface shown in Fig. 5b is made up of  $5 \times 5$ -order periodic unit cells. To test the operating principle, the unit cell is simulated using CST microwave studio software. Two alternative setups were used for the simulation. Two waveguide ports are situated on both sides of the unit cell in the X-direction in the first setup depicted in Fig. 2a. The second arrangement, depicted in Fig. 2b, features a unit cell in the Y-direction between two waveguide ports. Figure 3 shows the simulated effective permittivity and permeability obtained by simulation. It can be seen that the real value of permittivity in both simulation setups is negative across the whole simulation range, i.e. 1–10 GHz. Also from Fig. 4, the near zero refractive index is observed in both X-axis and Y-axis propagation.

Table 1  
Dimensions of the proposed unit cell

Parameter	Dimension (mm)	Parameter	Dimension (mm)
$s$	5.8	$s_1$	2.5
$s_2$	2.2	$s_3$	1.1
$s_4$	3	$s_5$	1
$s_6$	5	$s_7$	0.5

## III Antenna Design and Evolution

In the proposed antenna configuration, the top view of the proposed patch antenna is shown in Fig. 5a. The conventional antenna is made of FR-4, which has a dielectric constant of 4.6 and a thickness of 0.8 mm. The antenna consists of two concentric circle shaped patch with offset-fed coplanar waveguide (CPW). The inner circle is adorned with two arc-shaped patches. On the right side of the antenna, another arc-shaped patch is added to CPW feed.

The metasurface super-substrate is made up of unit cells by placing it in  $5 \times 5$ -order as shown in Fig. 5b. Figure 5c shows the 3-D view of the proposed antenna configuration. The optimized dimensions are listed in Table 2.

Table 2  
Dimensions of the proposed antenna

Parameter	Dimension (mm)	Parameter	Dimension (mm)
$w$	28	$w_1$	6.2
$w_2$	1.8	$w_3$	18
$w_4$	2.3	$w_u$	0.4
$w_t$	5.2	$t_1$	1
$t_2$	1	$t_3$	0.6
$l_1$	7	$l_2$	20
$l_3$	9	$r_1$	8
$r_2$	6.4	$h$	6

In Fig. 6, the evolution of the conventional patch antenna is graphically depicted in four different levels. Initially, a pair of concentric circles is fed using offset feeding technique. The corresponding  $S_{11}$

performance is depicted in Fig. 7. Next, the CPW feeding is employed in stage 2 and better  $S_{11}$  performance is observed when compared to stage 1. A pair of arc shaped patch is inserted inside the inner circle in stage 3. The stage 3 antenna provides one narrow band operation at 4.3 GHz and two wideband operations ranging from 5-6.1 GHz and 6.4–10.5 GHz. The final antenna is adorned with an arc shaped patch at the right side coplanar waveguide. This final design achieves the better performance as shown in Fig. 7.

## IV Results and Discussion

The proposed antenna with and without super-substrate is simulated using CST Microwave studio. The plot of frequency versus  $S_{11}$  of the proposed antenna configuration is plotted in Fig. 8. The antenna without super-substrate is simulated and observed two wideband operations. With a -10 dB impedance bandwidth of 65%, this antenna produces first wideband resonance from 3.1 GHz-6.1GHz. The second wideband operation ranges from 6.4 GHz-10.4 GHz with a -10 dB impedance bandwidth of 47%. After that, the simulation with the proposed metamaterial super-substrate is performed. In compared to the antenna without the super-substrate, the  $S_{11}$  performance suffers only little degradation. The two-layer antenna, on the other hand, has a substantially higher gain. Three wideband operations are visible in the final antenna design. Firstly, the antenna has an  $S_{11}$  of less than -10 dB from 3.1 to 4.5 GHz and a 39% impedance bandwidth. With an impedance bandwidth of 18%, the second wideband response is achieved between 5.1 and 6.15 GHz. Next, with an impedance bandwidth of 47%, wideband operation is found from 6.5 GHz to 10.5 GHz. Further investigation was carried out to determine the impact of various parameters on impedance bandwidth and return loss.

Initially, the effect of circle thickness on  $S_{11}$  performance is studied by varying  $t_1$ . It can be seen from the Fig. 9 that the antenna achieves optimum performance when  $t_1 = 1$  mm. On changing  $t_1$ , the resonance peak becomes weak in some frequency and bandwidth is also reduced. Figure 10 shows variation of  $S_{11}$  with respect to frequency on varying  $t_2$ . It can be observed that when  $t_2 = 1$  mm the antenna achieves better performance in terms of  $S_{11}$  and gain. Finally, the effect of length of the patch that connects the inner arcs ( $w_f$ ) is studied using simulation. The  $S_{11}$  performance for various values of  $w_f$  is plotted in Fig. 11. It is observed from the simulation results the antenna achieves better performance when  $w_f = 5.2$  mm.

Figure 12 shows the surface current distribution of the proposed patch antenna top surface at 3.5GHz, 4.2GHz, 5.5GHz, and 10.1GHz. At 3.5 GHz, the arc-shaped patch connected to the CPW feed exhibits a high intensity of current flow. Concentric circle-shaped patches provide the second resonance peak at 4.2 GHz. Also the current distribution at 5.5 and 10.1 GHz is high at the edges of the circles. The proposed antenna configuration is fabricated and measured. The front view of the patch and metasurface is shown in Fig. 13. The three dimensional view of the fabricated antenna is shown in Fig. 14a. The radiation pattern measurement has been performed in anechoic chamber as shown in Fig. 14b. The antenna with and without metamaterial super-substrate is considered for measurement. Anritsu Vector Network Analyzer was used to test the antenna prototype. The corresponding results are plotted in Fig. 15. It is

found from Fig. 15, the experimentally measured  $S_{11} < -10\text{dB}$  without super-substrate has been achieved from 3.0 GHz to 10.3 GHz with an impedance bandwidth of 109%. The measured  $S_{11}$  for the proposed antenna with super-substrate exhibits three wideband responses, i.e. 3.06GHz – 4.72GHz (B.W of 42%), 4.94GHz-6.19GHz (B.W of 22%) and 6.50 GHz – 10.56 GHz (B.W of 47.5%). The discrepancies between simulated and measured results might have been occurred due to fabrication tolerances.

The proposed antenna's simulated and measured gains are almost identical as shown in Fig. 16. The addition of a metasurface to a simple conventional patch results in a gain enhancement of 6.2 dBi in the developed antenna. The proposed antenna's radiation pattern characteristics in the E-plane and H-plane have been measured in the anechoic chamber and shown in Fig. 17 and Fig. 18, respectively. At 3.5 GHz, 4.2 GHz, 5.5 GHz, and 10.1 GHz, the radiation characteristics of the proposed antenna arrangement are simulated and measured. Radiation from the antenna is stable in all directions.

Table 3 compares the proposed antenna's performance to that of some of the previously reported high-performance antennas. According to the findings, the proposed low profile design has significantly increased gain while reducing size.

Table 3  
Comparison of the proposed antenna with the existing antennas

Reference	Dimension (mm)	Maximum Bandwidth (%)	Max. Gain (dBi)	Operating frequency (GHz)
[12]	28 × 28	19%	7.57	9.24–11.25
[22]	78.6 × 42.5	28%	6.72	(0.865–1.060), (2.240–2.520), (3.250–4.310), (4.900–6.500)
[23]	28.8 × 32	126%	7.3	3-13.25
[24]	48 × 48	13%	4.72	(1.710–1.880), (1.880–2.200), (3.400–3.800)
[25]	67.2 × 67.2	16.58%	12	9.4–11.2
Proposed work	28 × 28	47.5%	6.2	(3.06–4.72), (4.94–6.19), (6.5–10.5)

# V Conclusion

The gain enhancement of a metamaterial super-substrate loaded concentric circle shaped antenna fed by coplanar waveguide has been studied. The antenna can operate in three wideband modes: 3.06GHz-4.72GHz (B.W of 42%), 4.94GHz-6.19GHz (B.W of 22%), and 6.50GHz-10.56GHz (B.W of 47.5% ). The proposed layered antenna achieves considerable gain enhancement of 181% at X-band with a maximum gain of 6.2 dBi using a  $5 \times 5$  order configuration of the proposed unit cell. The proposed metasurface's near-zero refractive index, as demonstrated by simulation, increases gain over a wide range of operations. The experimental results reveal that the super-substrate-based antenna has the needed impedance bandwidth for WLAN, LTE-A, 5G Wi-Fi, and X-band applications.

## Declarations

### Statements & Declarations

*"The authors declare that no funds, grants, or other support were received during the preparation of this manuscript."*

### Competing Interests

*"The authors have no relevant financial or non-financial interests to disclose."*

### Author Contributions

A.Sujatha Priyadarshini has contributed to the basic design simulation and fabrication. C.Arvind and Madurakavi karthikeyan contributed the performance enhancement and manuscript preparation.

### Data Availability

There is no dataset available for this project

## References

1. Mak, Angus CK, Corbett R. Rowell, Ross D. Murch, and Chi-Lun Mak. "Reconfigurable multiband antenna designs for wireless communication devices." *IEEE Transactions on Antennas and Propagation* 55, no. 7 (2007): 1919-1928.
2. Lee, Seung-hyun, and Youngje Sung. "Multiband antenna for wireless USB dongle applications." *IEEE Antennas and Wireless Propagation Letters* 10 (2011): 25-28.
3. G. Feng, L. Chen, X. Xue and X. Shi, "Broadband Surface-Wave Antenna With a Novel Nonuniform Tapered Metasurface," *IEEE Antennas and Wireless Propagation Letters*, Vol. 16, pp. 2902-2905, 2017.
4. W. Liu, Z. N. Chen, and X. M. Qing, "Metamaterial-based low-profile broadband aperture-coupled grid-slotted patch antenna," *IEEE Trans. Antennas Propag.*, vol. 63, no. 7, pp. 3325–3329, Jul. 2015.

5. F. H. Lin and Z. N. Chen, "Low-profile wideband metasurface antennas using characteristic mode analysis," *IEEE Trans. Antennas Propag.*, vol. 65, no. 4, pp. 1706–1713, Apr. 2016
6. Smith, David R., Okan Yurduseven, Laura Pulido Mancera, Patrick Bowen, and Nathan B. Kundtz. "Analysis of a waveguide-fed metasurface antenna." *Physical Review Applied* 8, no. 5 (2017): 054048.
7. J. Wang, H. Wong, Z. Ji and Y. Wu, "Broadband CPW-Fed Aperture Coupled Metasurface Antenna," in *IEEE Antennas and Wireless Propagation Letters*, vol. 18, no. 3, pp. 517-520, March 2019.
8. Caloz C, Itoh T, *Electromagnetic Metamaterials: Transmission Line Theory and Microwave Applications*, John Wiley & Sons, 2006, Inc
9. Arbabi, Amir, Ehsan Arbabi, Yu Horie, Seyedeh Mahsa Kamali, and Andrei Faraon. "Planar metasurface retroreflector." *Nature Photonics* 11, no. 7 (2017): 415-420.
10. Ziolkowski, Richard W. "Design, fabrication, and testing of double negative metamaterials." *IEEE Transactions on antennas and Propagation* 51, no. 7 (2003): 1516-1529.
11. Hossain, Md Iqbal, Mohammad Rashed Iqbal Faruque, Mohammad Tariqul Islam, and Mohammad Habib Ullah. "A new wide-band double-negative metamaterial for C-and S-band applications." *Materials* 8, no. 1 (2015): 57-71.
12. Samantaray, Diptiranjana, and Somak Bhattacharyya. "A gain-enhanced slotted patch antenna using metasurface as superstrate configuration." *IEEE Transactions on Antennas and Propagation* 68, no. 9 (2020): 6548-6556.
13. Y. Zheng et al., "Wideband Gain Enhancement and RCS Reduction of Fabry–Perot Resonator Antenna With Chessboard Arranged Metamaterial Superstrate," in *IEEE Transactions on Antennas and Propagation*, vol. 66, no. 2, pp. 590-599, Feb. 2018.
14. Islam, M., Islam, M., Samsuzzaman, M., Faruque, M., Misran, N., Mansor, M. "A miniaturized antenna with negative index metamaterial based on modified SRR and CLS unit cell for UWB microwave imaging applications". *Materials* 2015, vol. 8, pp.392–407.
15. Dong, Y., Itoh, T. *Metamaterial-based antennas*. Proc. IEEE 2012, vol. 100, pp. 2271–2285
16. Zhu, C., Ma, J.-J., ; Zhai, H.-Q., Li, L., Liang, C.-H. "Characteristics of electrically small spiral resonator metamaterial with electric and magnetic responses". *IEEE Antennas Wirel. Propag. Lett.* 2012, 11, 1580–1583.
17. Su, L, Naqui, J., Mata-Contreras, J., Martín, F. "Modeling and applications of metamaterial transmission lines loaded with pairs of coupled complementary split-ring resonators (CSRRs)". *IEEE Antennas Wirel. Propag. Lett.* 2016, 15, 154–157.
18. Kim, O.S., Breinbjerg, O. "Miniaturised self-resonant split-ring resonator antenna" . *Electron. Lett.* 2009, vol. 45, pp 196–197.
19. Engheta, N.; Ziolkowski, R.W. *Metamaterials: Physics and Engineering Explorations*; John Wiley & Sons: Hoboken, NJ, USA, 2006.

20. Hasan, M.M.; Faruque, M.R.I.; Islam, M.T. Left-handed meta-surface loaded with ring resonator modelling for satellite application. *Int. J. Satell. Commun. Netw.* 2018, 36, 352–360. b]. *J. Electromagn. Anal. Appl.* 2015, 7, 276.
21. Wang, J.-J.; Gong, L.-L.; Sun, Y.-X.; Zhu, Z.-P.; Zhang, Y.-R. High-gain composite microstrip patch antenna with the near-zero-refractive-index metamaterial. *Opt. Int. J. Light Electron. Opt.* 2014, 125, 6491–6495.
22. Samir Salem Al-Bawri et al. “Metamaterial Cell-Based Superstrate towards Bandwidth and Gain Enhancement of Quad-Band CPW-Fed Antenna for Wireless Applications” , *Sensors* 2020, 20, 457
23. Kumar, S, Kumari, R. “Composite right/left-handed ultra-wideband metamaterial antenna with improved gain”, *Microw Opt Technol Lett.* 2021, vol. 63, pp. 188– 195.
24. Ameen, M., Chaudhary, R.K. “Dual-layer and Dual-polarized Metamaterial Inspired Antenna using Circular-Complementary Split Ring Resonator Mushroom and Metasurface for Wireless Applications”. *AEU Int. J. Electron. Commun*, 2019, vol. 113, pp. 152977.
25. Y. Zheng et al., "Wideband Gain Enhancement and RCS Reduction of Fabry–Perot Resonator Antenna With Chessboard Arranged Metamaterial Superstrate," in *IEEE Transactions on Antennas and Propagation*, vol. 66, no. 2, pp. 590-599, Feb. 2018.

## Figures

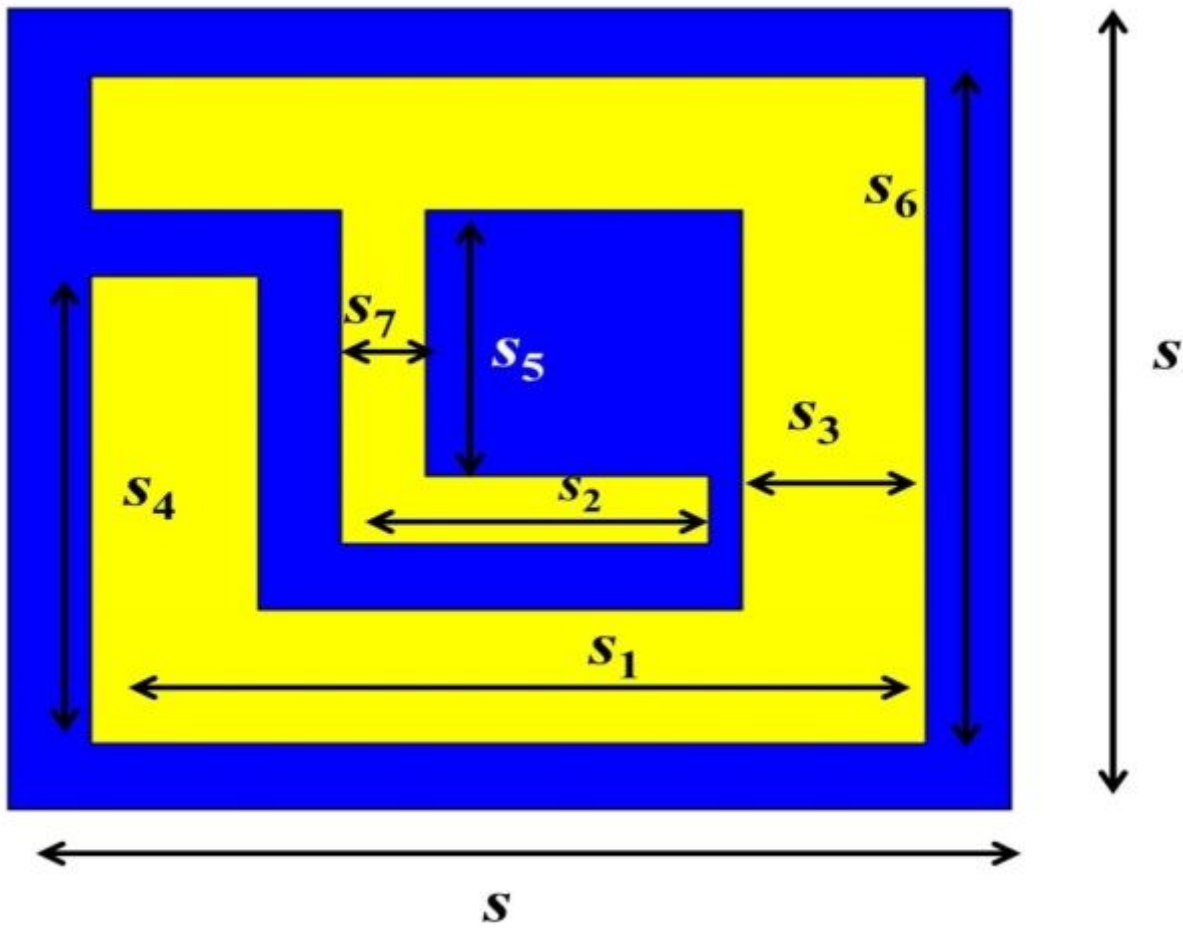


Figure 1

*Structure of the proposed unit cell*

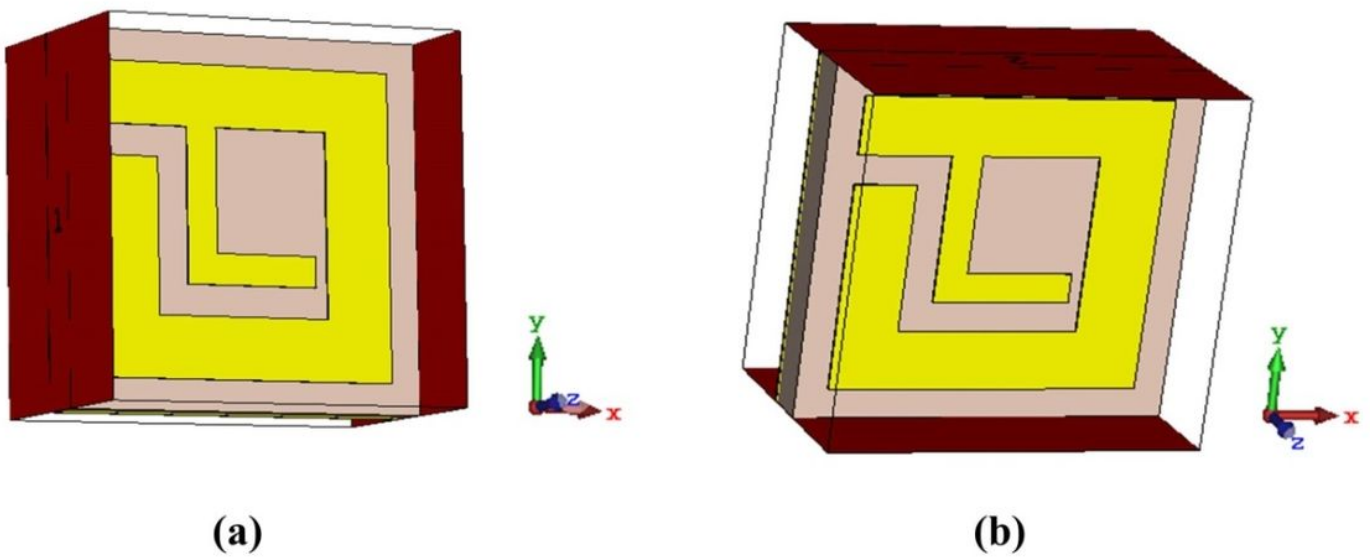


Figure 2

Unit cell simulation setup in (a) x-direction and (b) y-direction

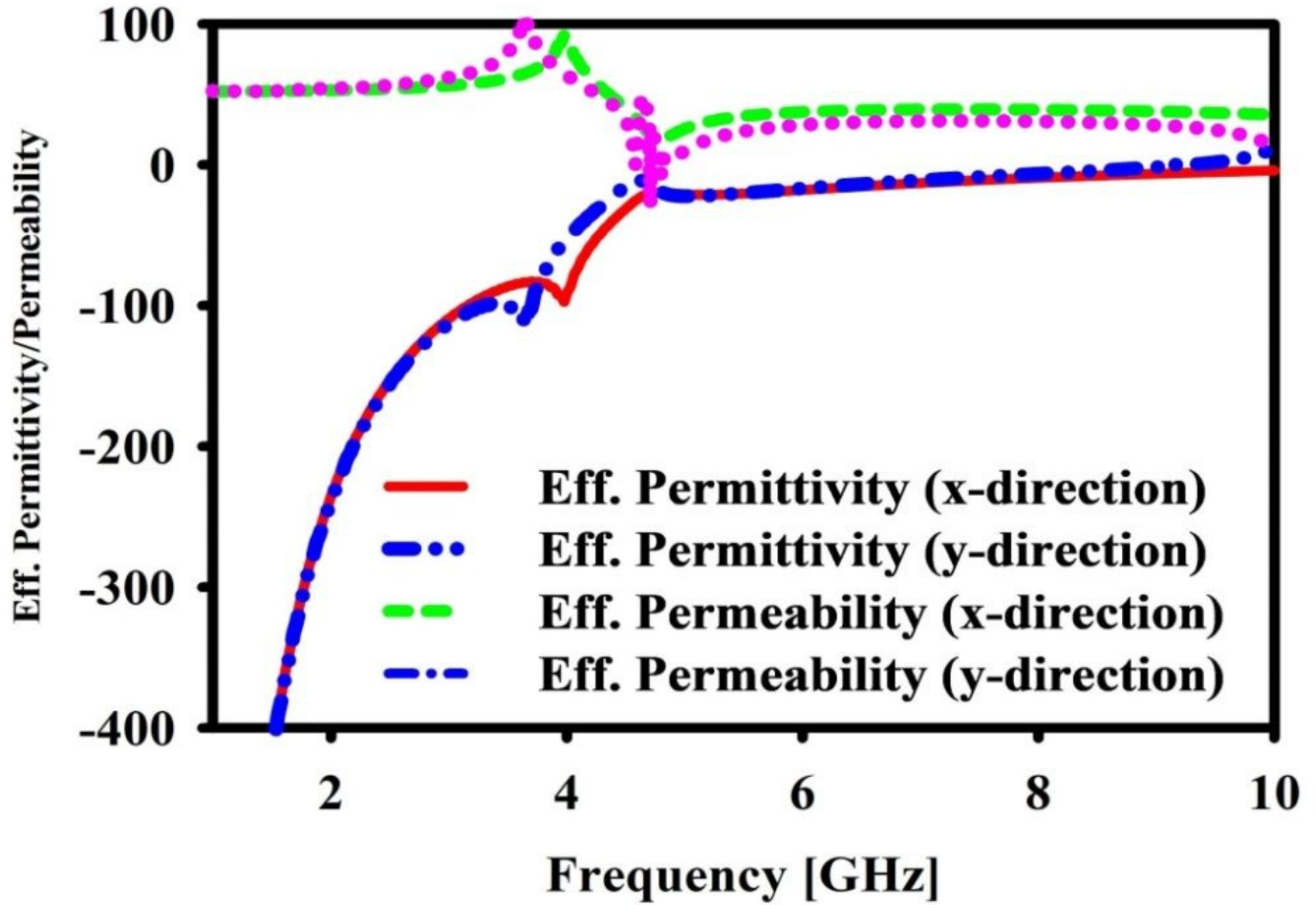


Figure 3

Simulated permittivity and permeability of proposed unit cell in x and y – direction

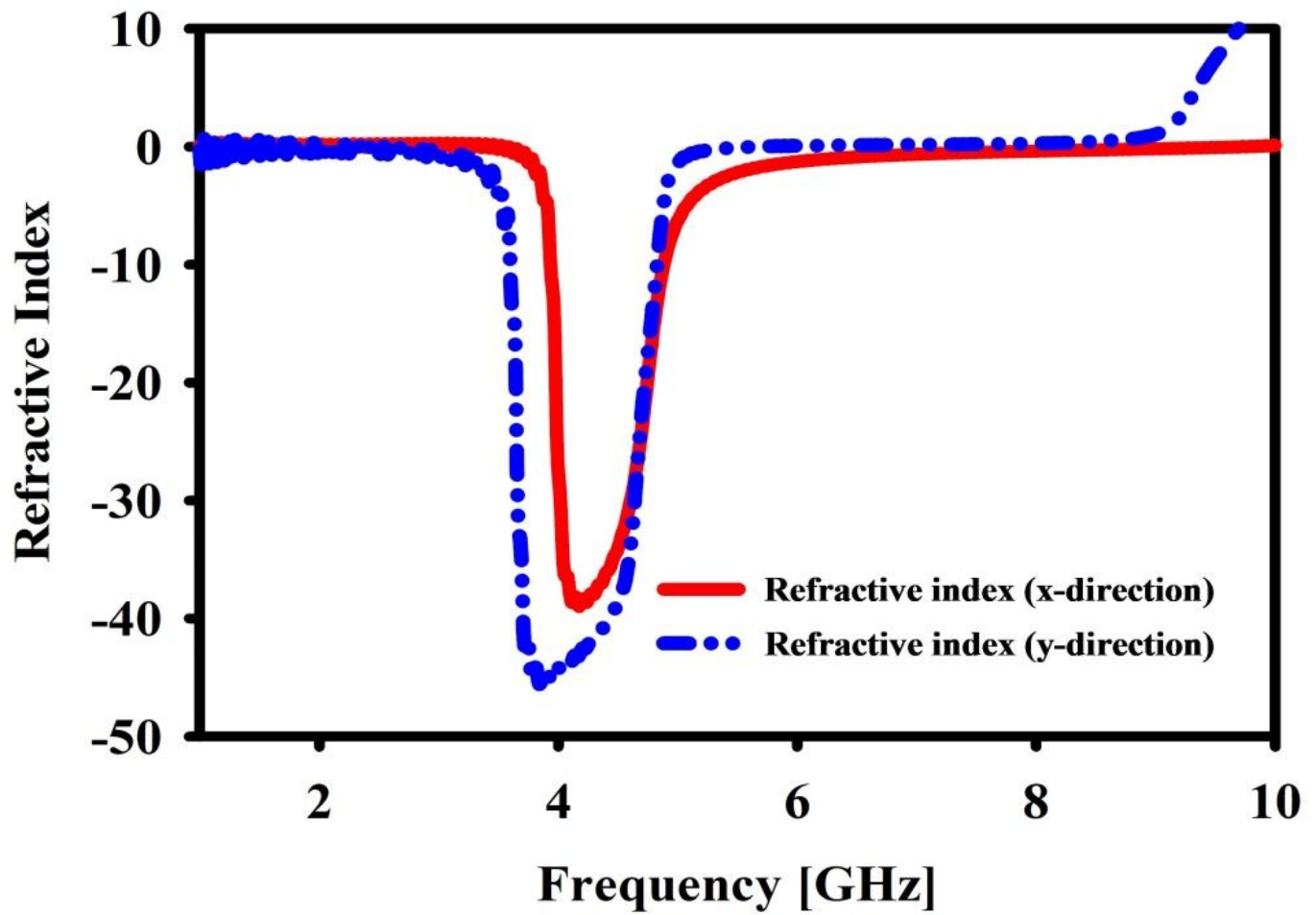
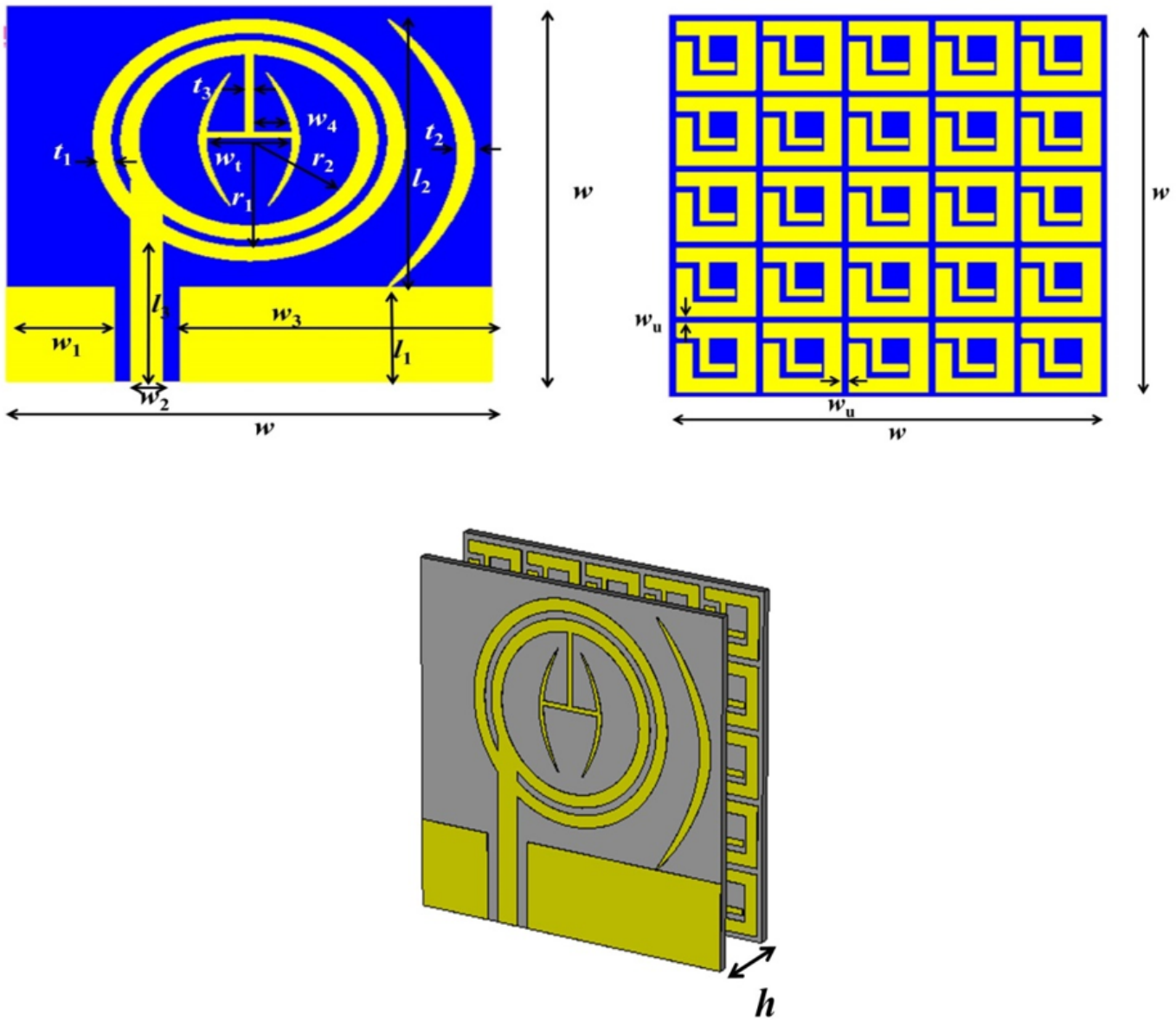


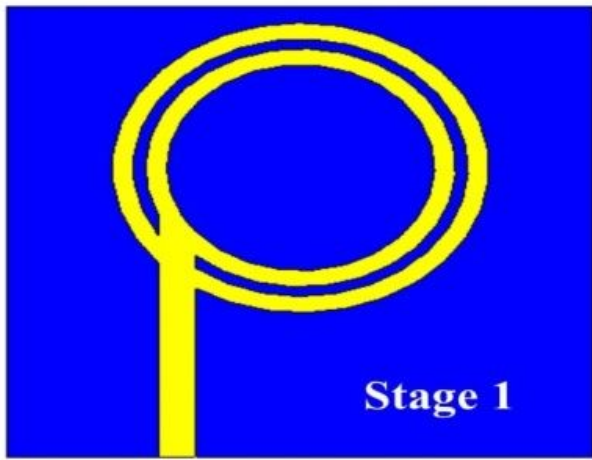
Figure 4

*Simulated refractive index of the proposed metamaterial structure*

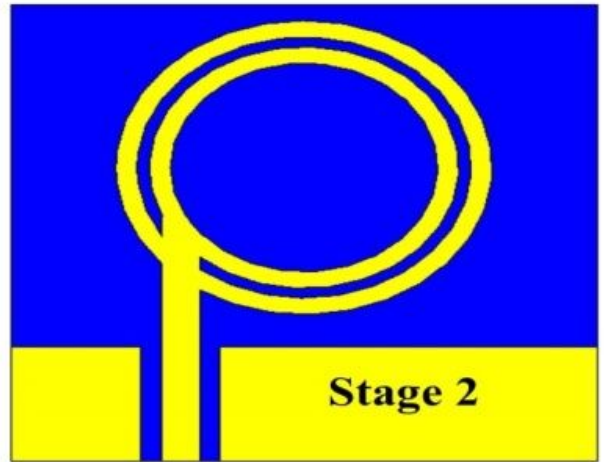


**Figure 5**

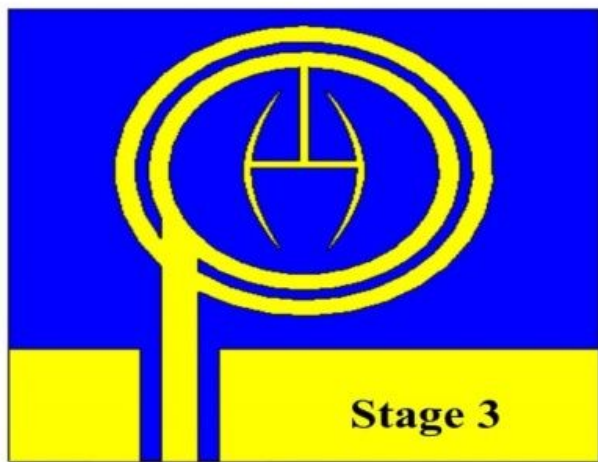
*(a) Design of the proposed patch antenna, (b) Structure of the metasurface super-substrate and (c) 3D view of the proposed antenna configuration*



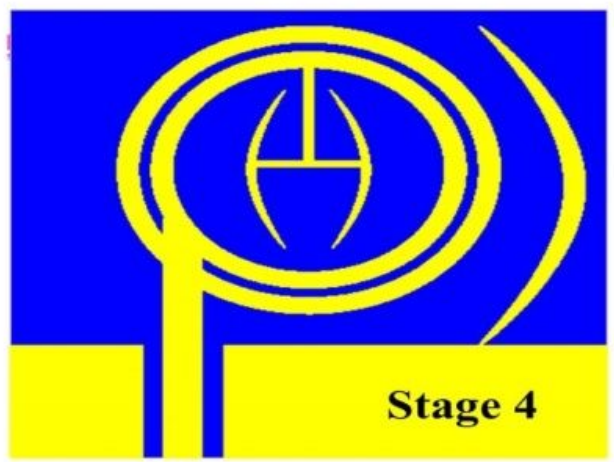
(a)



(b)



(c)



(d)

Figure 6

*Development stages of the proposed antenna*

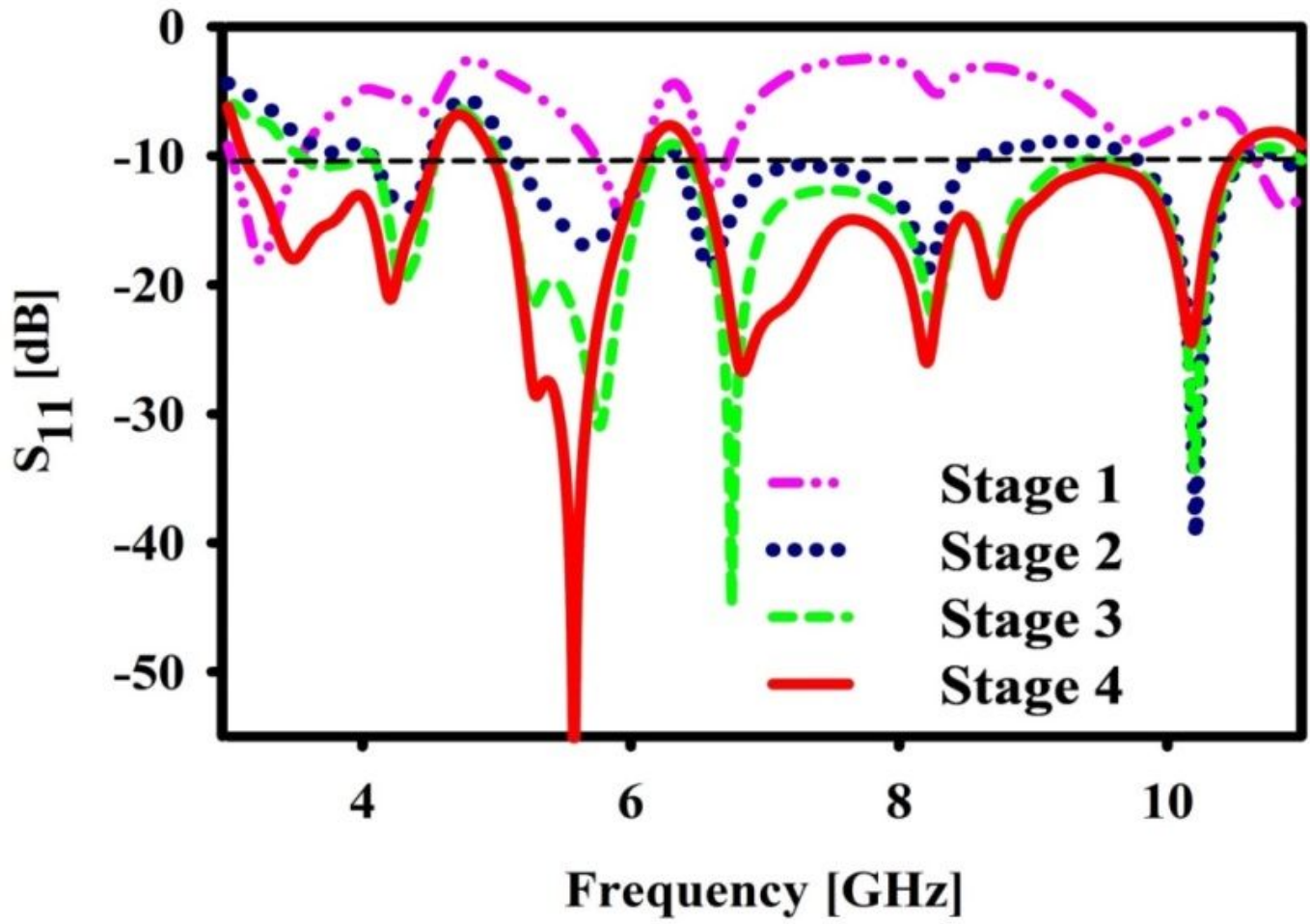


Figure 7

*Evolution stages  $S_{11}$  performance of the proposed antenna*

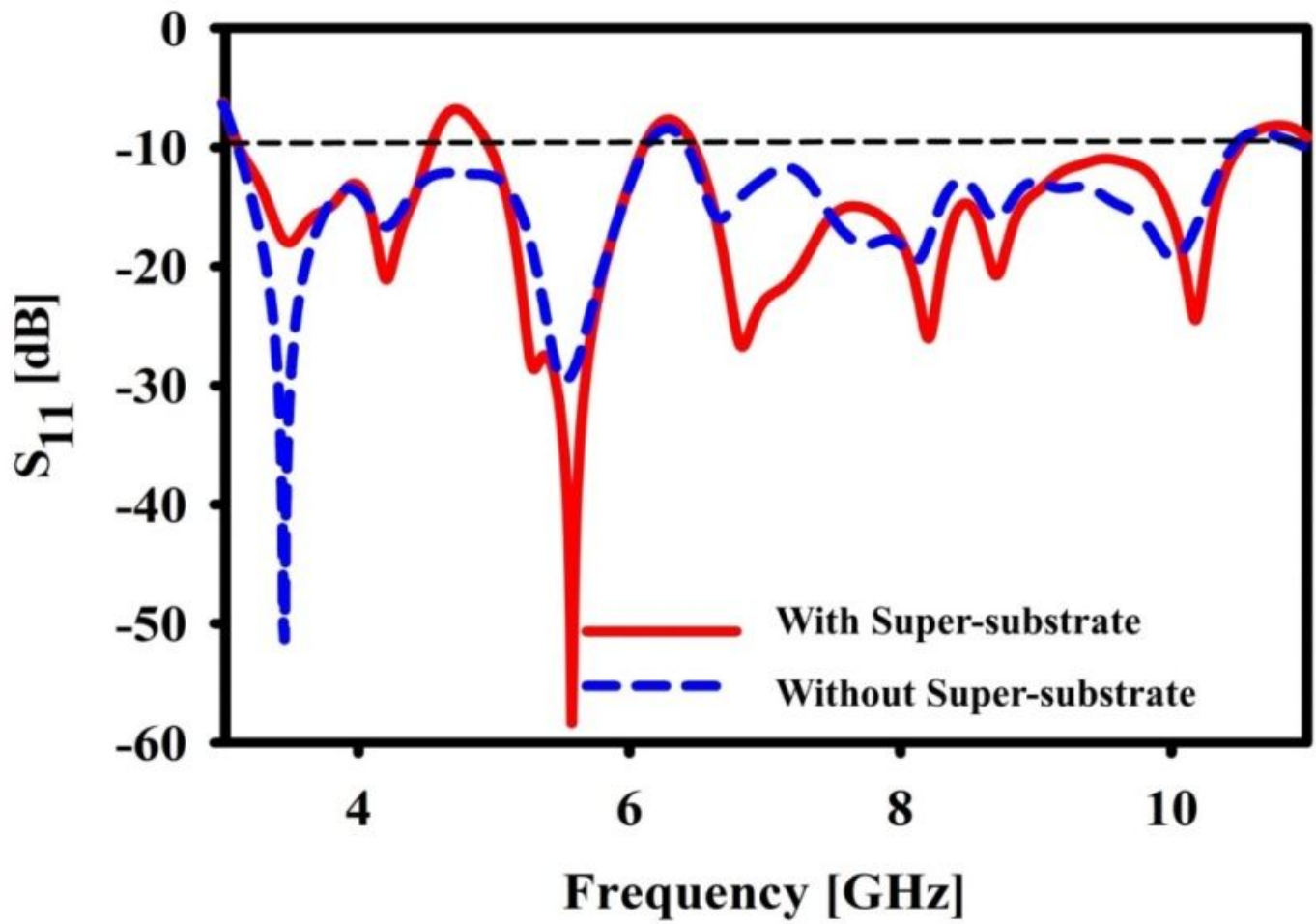


Figure 8

*Comparison of  $S_{11}$  of the proposed antenna configuration with and without metamaterial super-substrate*

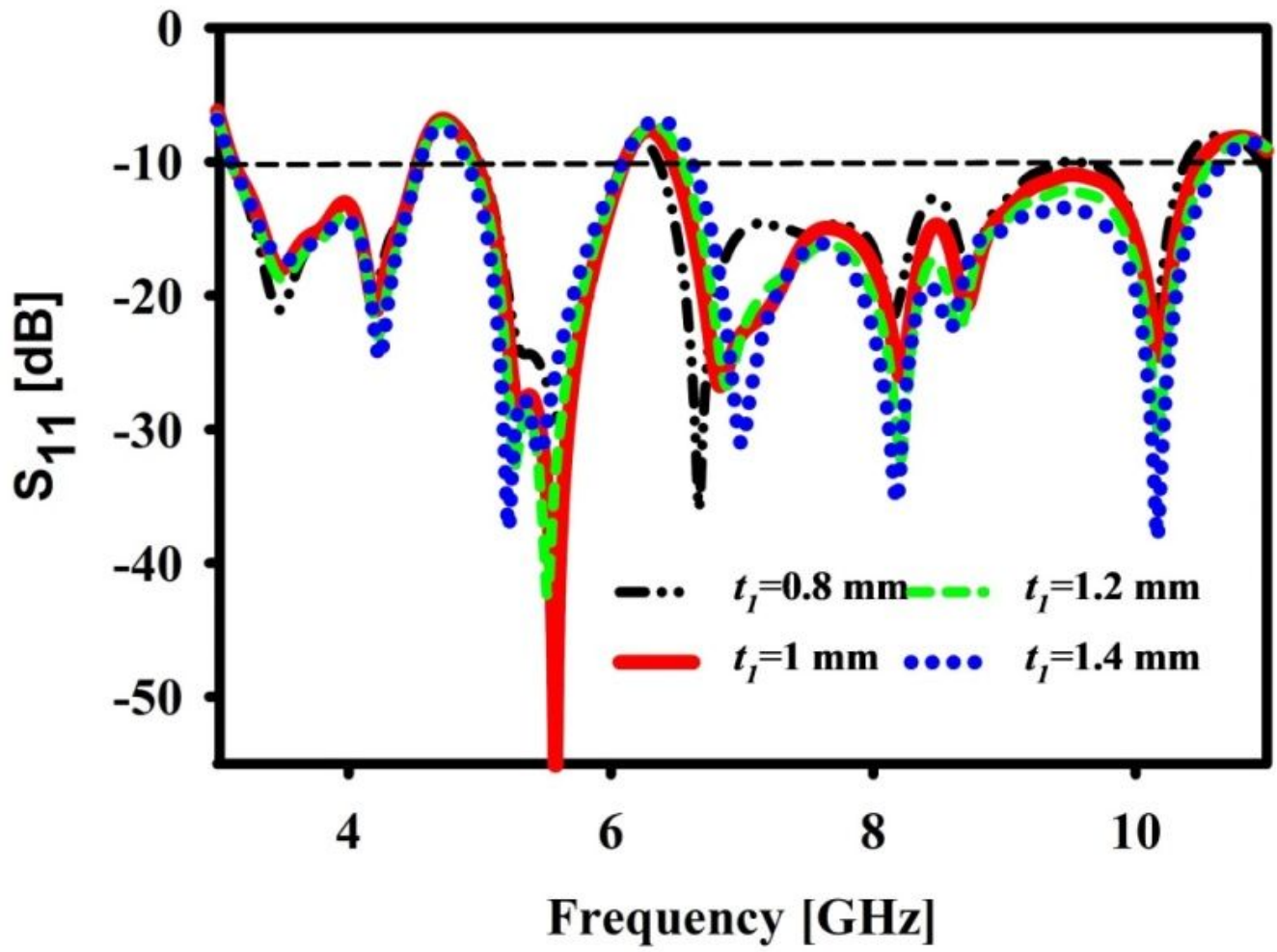


Figure 9

Variation of  $S_{11}$  with the variation in  $t_1$

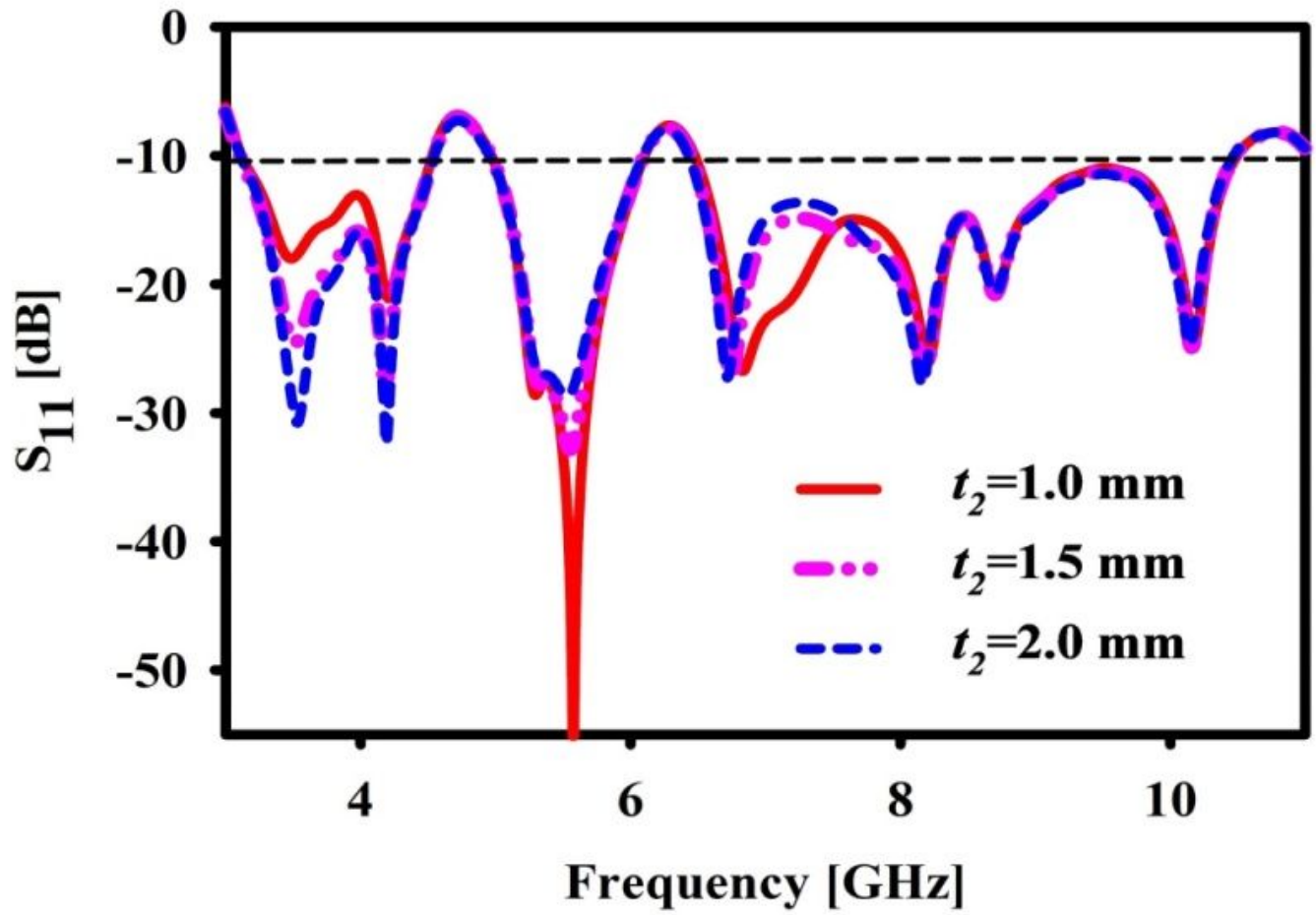


Figure 10

*Variation of  $S_{11}$  with the variation in  $t_2$*

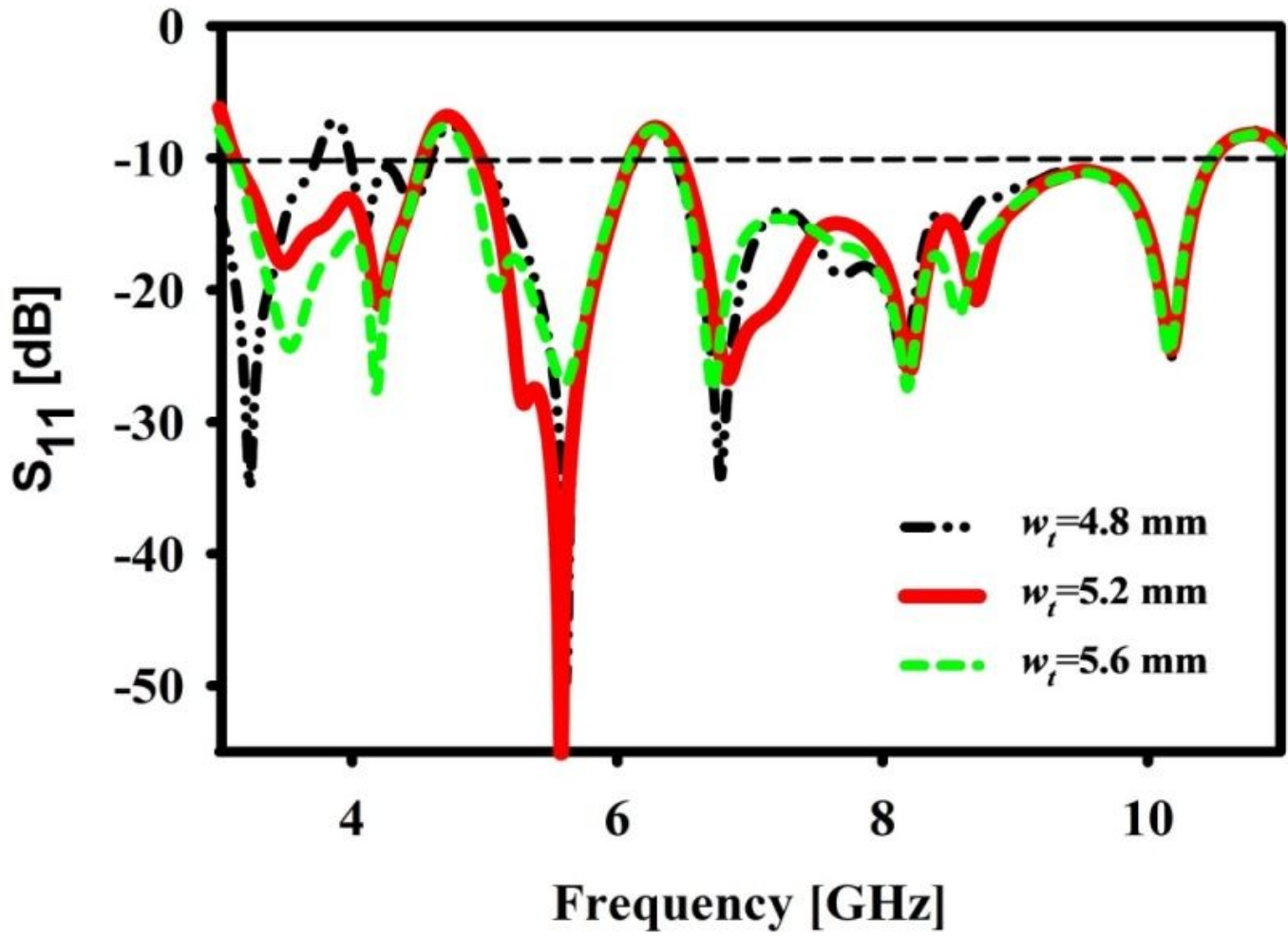


Figure 11

*Effect of  $w_t$  on the  $S_{11}$  performance of the proposed antenna*

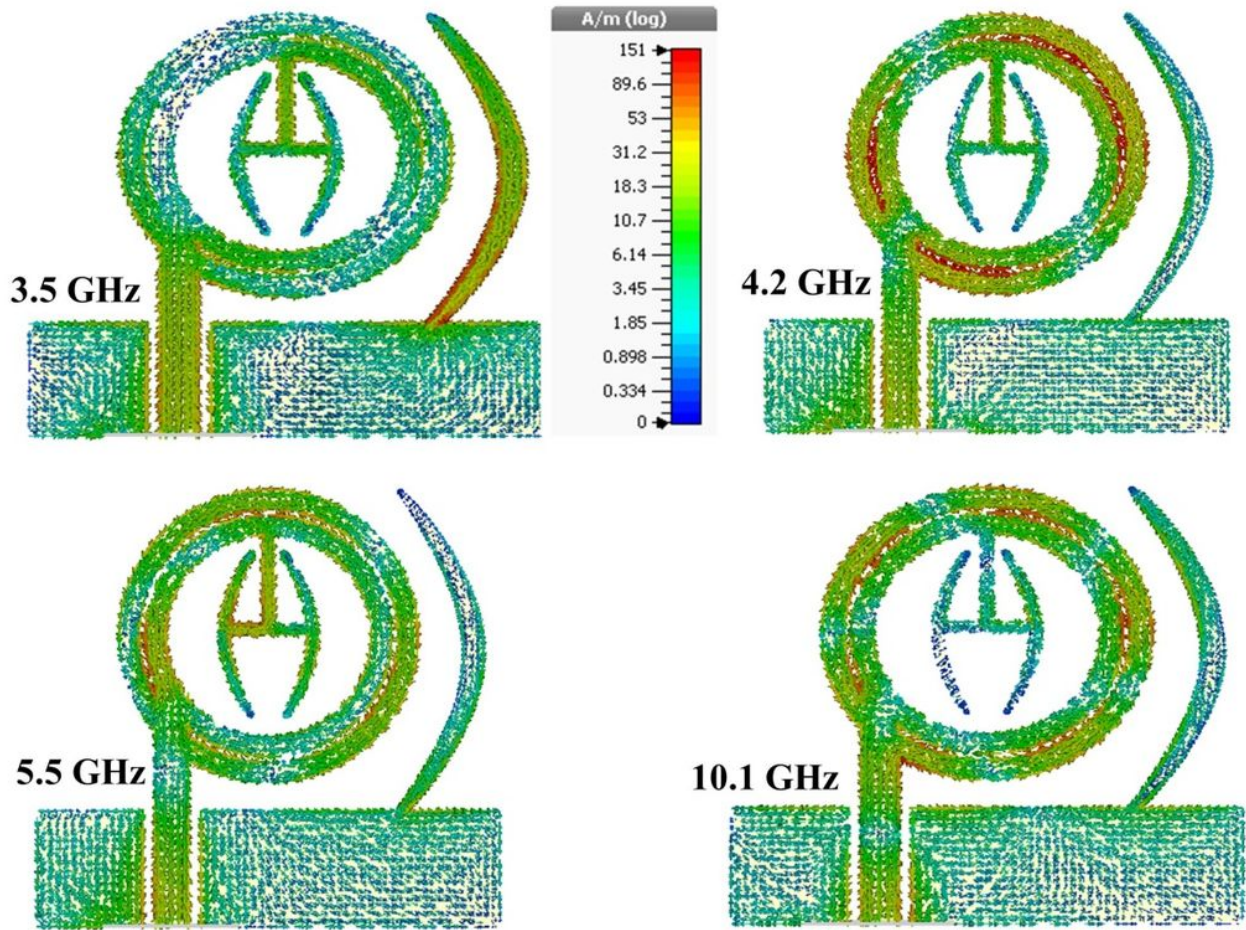
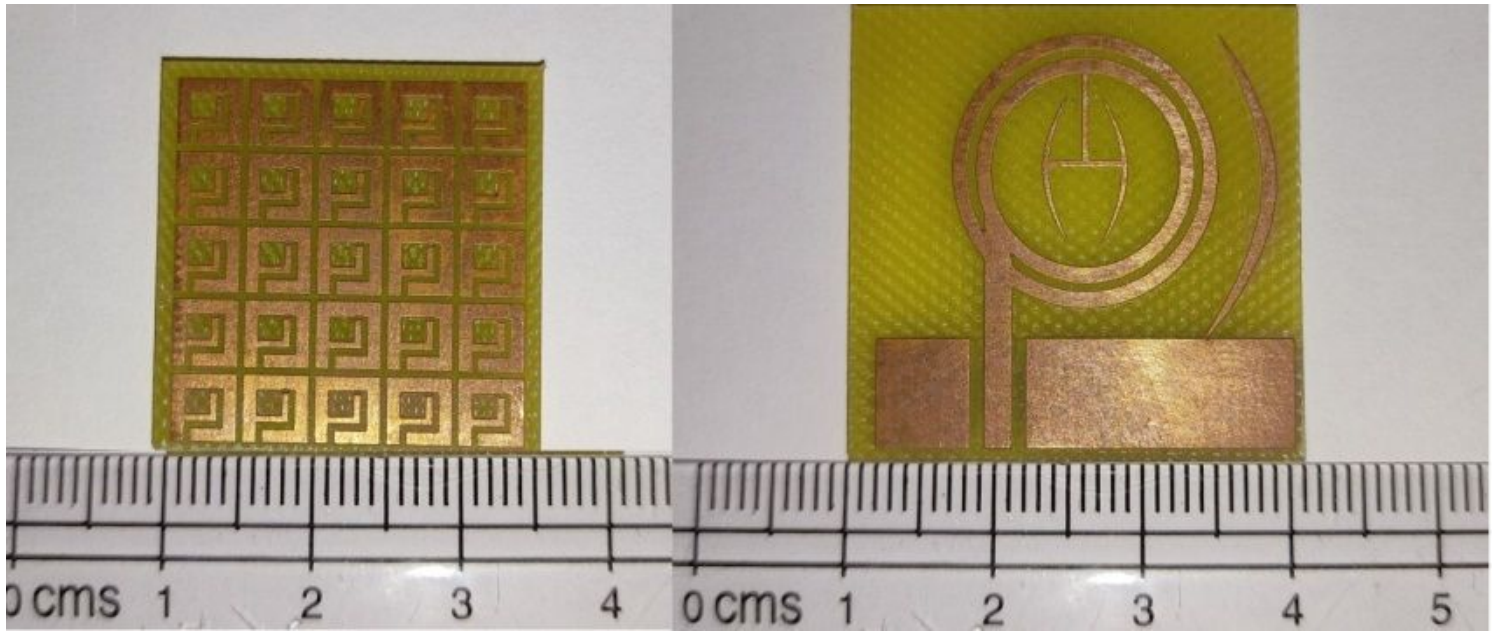


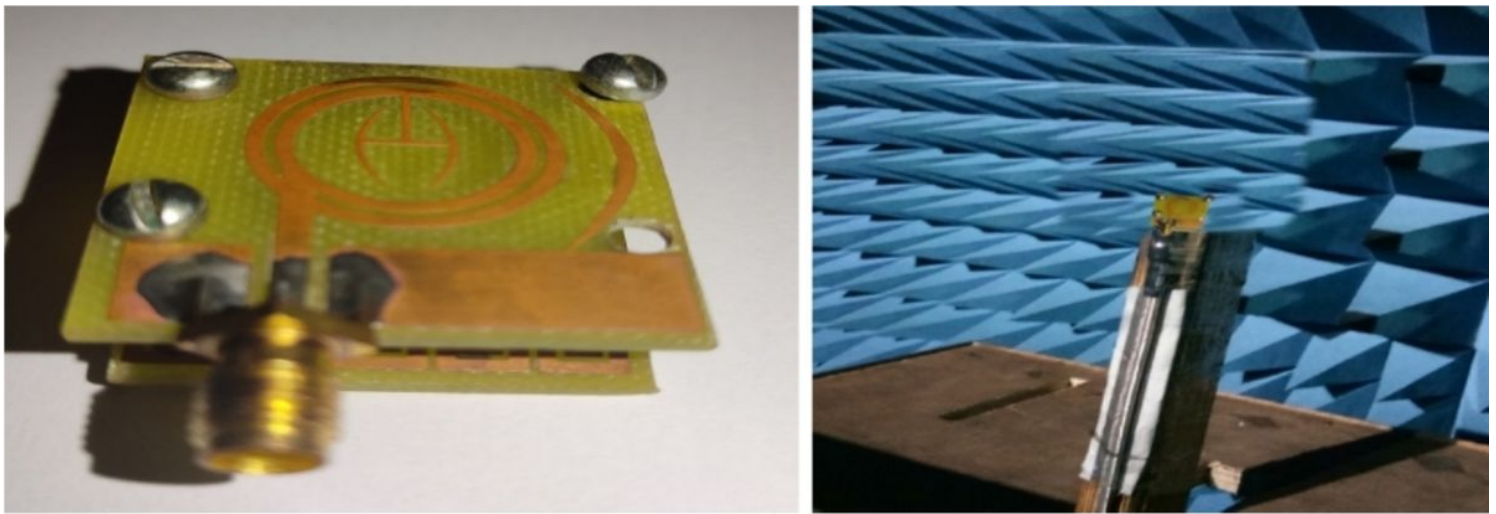
Figure 12

*Surface current distribution of the proposed antenna at various frequencies*



**Figure 13**

Fabricated prototype of the proposed antenna



(a) (b)

**Figure 14**

(a) 3-D view of the fabricated antenna (b) Anechoic chamber measurement setup

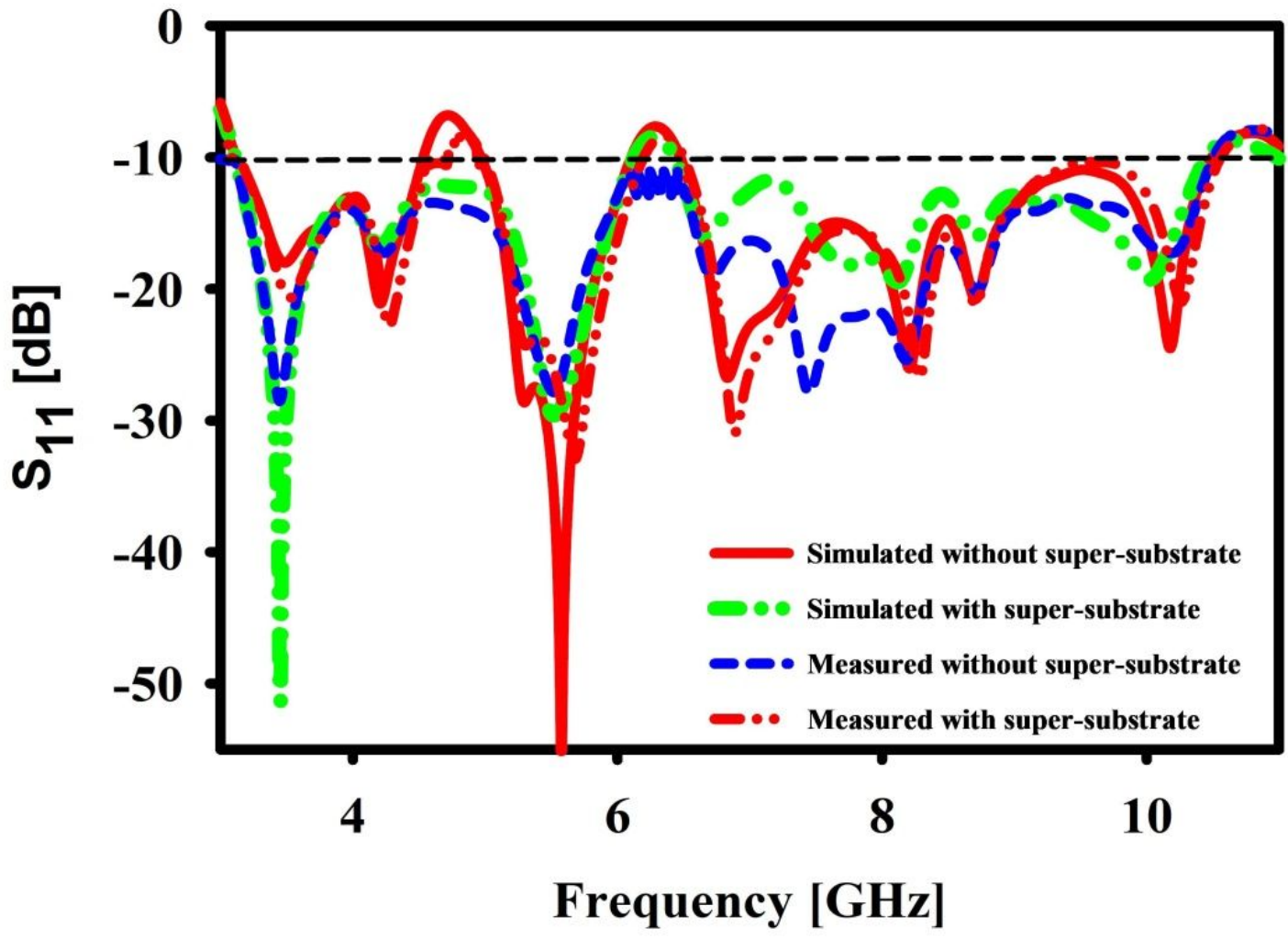


Figure 15

Simulated and measured  $S_{11}$  of the proposed antenna configurations

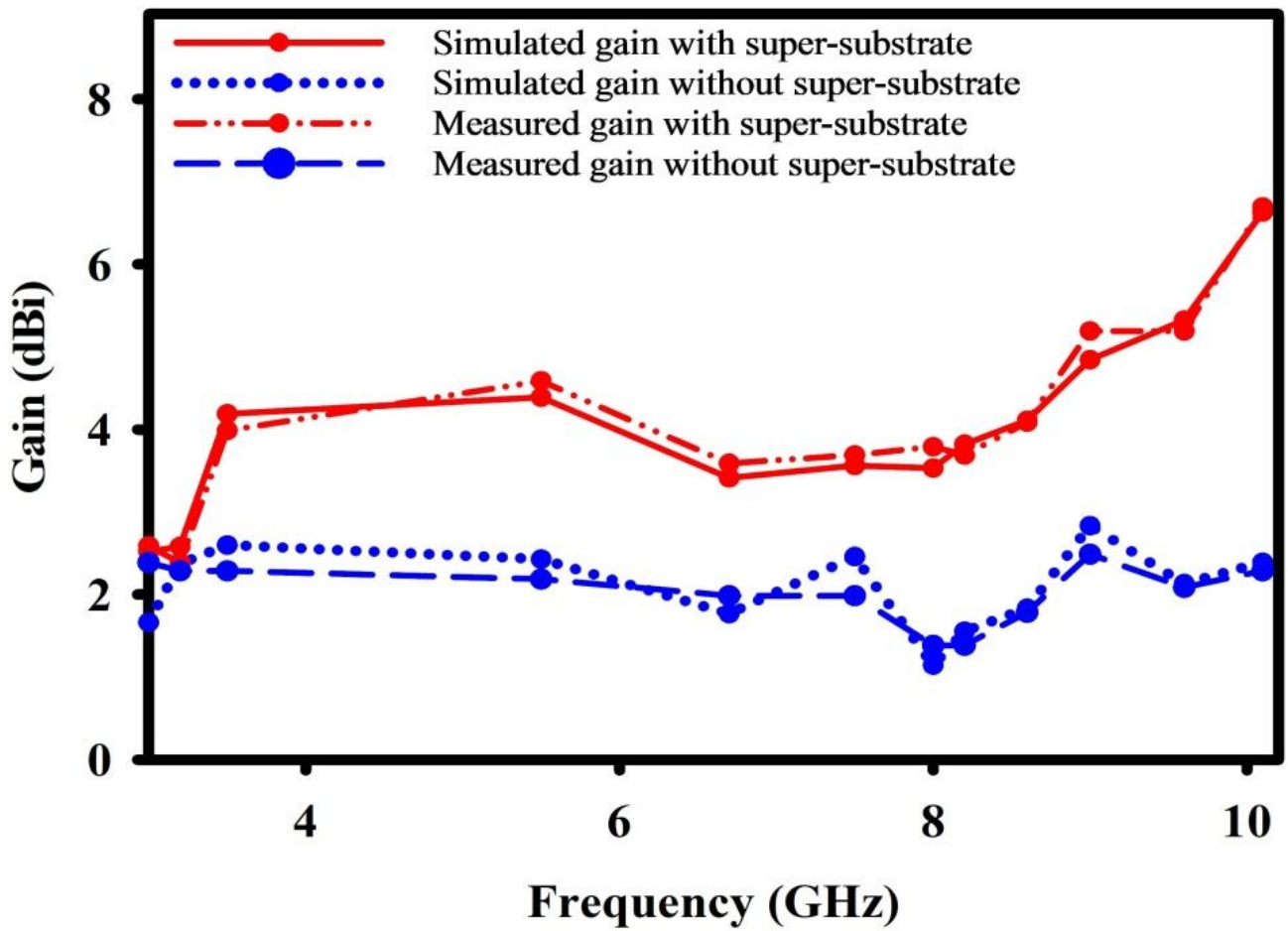


Figure 16

*Simulated and measured gain of the proposed antenna configurations*

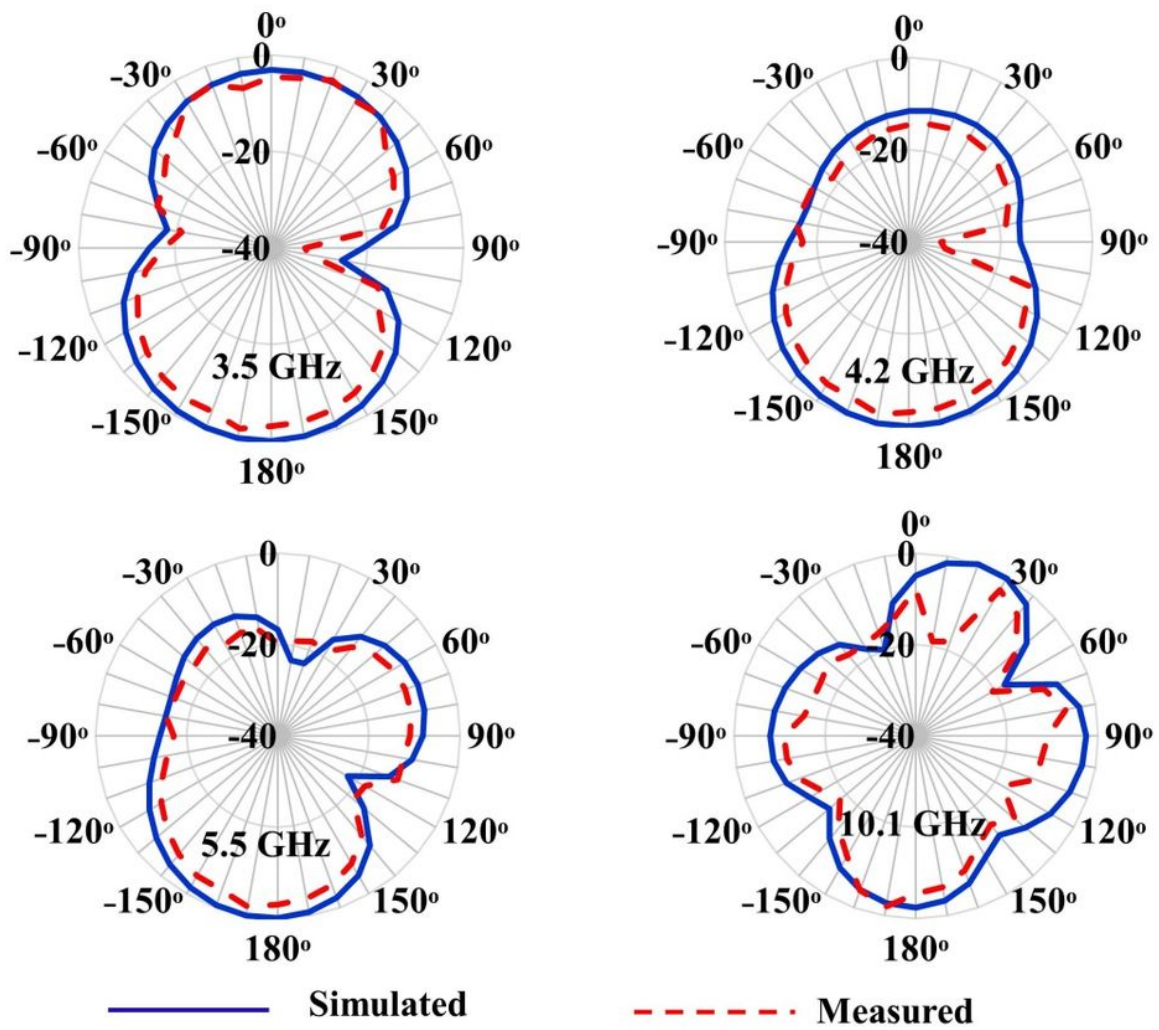
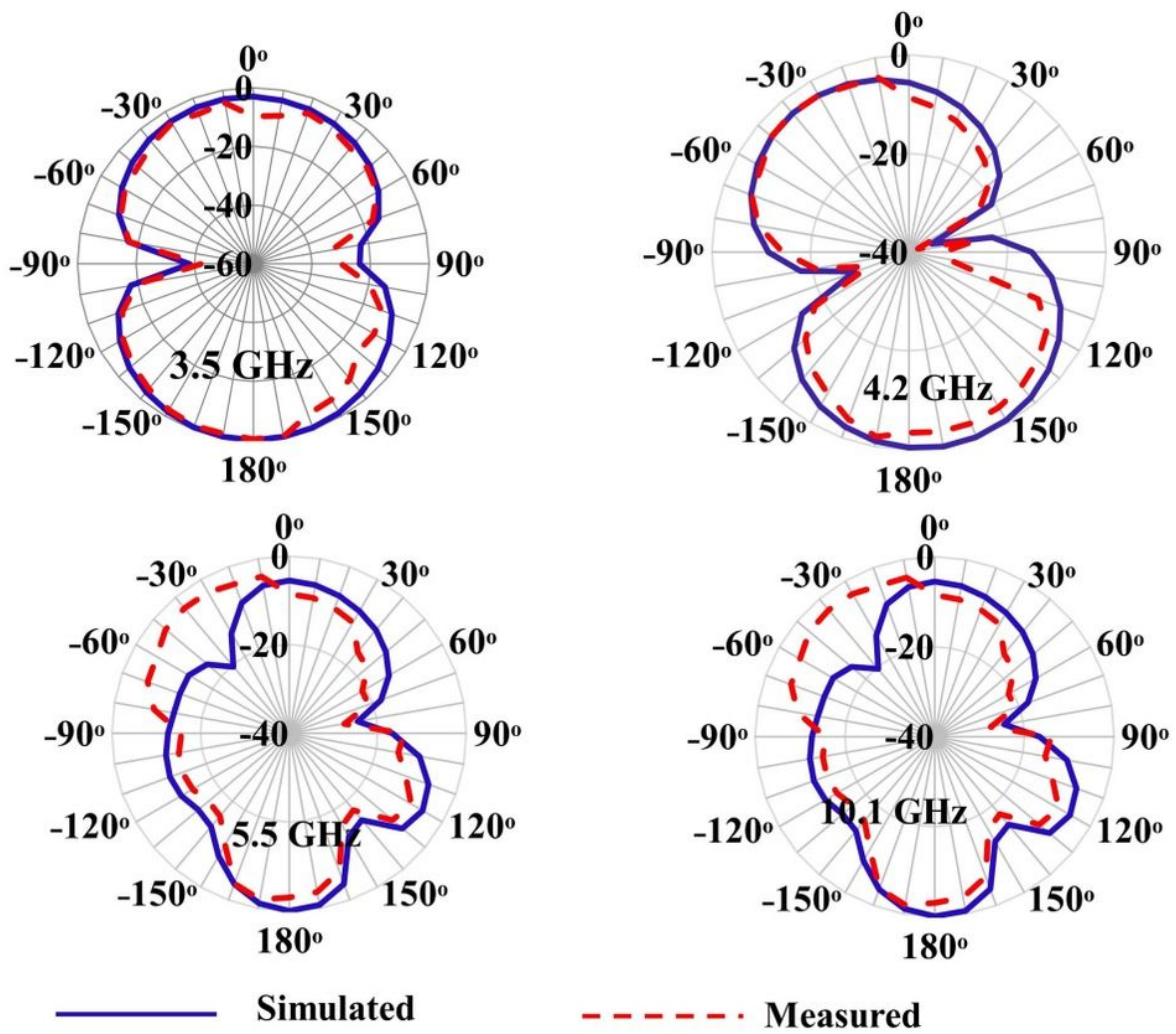


Figure 17

Simulated and measured E-plane radiation pattern of the proposed antenna configuration



**Figure 18**

*Simulated and measured H-plane radiation pattern of the proposed antenna configuration*